Chemical Engineering Journal 151 (2009) 220–227

Contents lists available at ScienceDirect

Chemical Engineering Journal

journal homepage: www.elsevier.com/locate/cej

Flame sprayed V-doped TiO_2 nanoparticles with enhanced photocatalytic activity under visible light irradiation

Baozhu Tian[a,b], Chunzhong Li[a,*], Feng Gu[a], Haibo Jiang[a], Yanjie Hu[a], Jinlong Zhang[b]

[a] Key Laboratory for Ultrafine Materials of Ministry of Education, School of Materials Science and Engineering, East China University of Science and Technology, Meilong Road, Shanghai 200237, PR China
[b] Laboratory for Advanced Materials, Institute of Fine Chemicals, East China University of Science and Technology, Meilong Road, Shanghai 200237, PR China

ARTICLE INFO

Article history:
Received 15 October 2008
Received in revised form 23 February 2009
Accepted 25 February 2009

Keywords:
Titanium dioxide
Nanoparticles
Flame spray pyrolysis
Photocatalytic activity
V doping

ABSTRACT

V-doped TiO_2 (V–TiO_2) nanoparticles were prepared by a simple one-step flame spray pyrolysis (FSP) technique. The obtained samples were characterized by X-ray diffraction (XRD), transmission electron microscopy (TEM), electron paramagnetic resonance (EPR) spectra, UV–vis absorption spectroscopy, and nitrogen adsorption–desorption methods. Benefiting from the short residence time and high quenching rate during the flame spray process, V^{4+} ions are successfully incorporated into the crystal lattice of TiO_2. It reveals that V doping favors the primary particle size growth as well as the increase of rutile content in the products. The photocatalytic activity of the V–TiO_2 samples under UV and visible light irradiation were evaluate by the photocatalytic degradation of methylene blue (MB) and 2,4-dichlorophenol (2,4-DCP), respectively. It was found that V doping enhances the photocalytic activity under both UV and visible light irradiation. Especially, under visible light irradiation, the degradation rate of 2,4-dichlorophenol over 1%V–TiO_2 is two times higher than that over undoped TiO_2. The photocatalytic mechanisms for V–TiO_2 samples under UV and visible light irradiation were tentatively discussed.

1. Introduction

Industry development is pervasively connected with the disposal of a large number of various toxic pollutants, which are harmful to the environment, hazardous to human health, and difficult to degrade by natural means [1]. During recent decades, applying TiO_2 photocatalyst to completely mineralize organic contaminants in wastewater and air has received much research attention owing to its favorable physical/chemical properties, low-cost, chemical stability, and non-toxicity [2–4]. However, because of the wide band gap of TiO_2, only a small UV fraction of solar light (3–5%) can be used to initiate photochemical reaction, resulting in a loss of energy efficiency [5,6]. Therefore, the effective utilization of visible light becomes one of the most important subjects for developing the future generation of TiO_2-based photocatalysts.

Doping with transition metals such as Fe, V, Mo, Co and Cr is one of the most effective approaches for synthesizing visible light-active photocatalysts [7–14]. It has been considered that the metal ions incorporated into TiO_2 crystal lattice can modify the electron properties of TiO_2, extending its light absorption in the visible light region [12,13]. As one of the typical transition metals, V has been frequently investigated because it can lead to conspicuous absorption in the visible region [11–18]. Up to now, many methods such as sol–gel [19], coprecipitation [20,21], wet impregnation [21], liquid phase deposition [18], and ion-implantation methods [13,14] have been established for synthesizing V–TiO_2 catalysts. Among these preparation techniques, sol–gel and coprecipitation require further heat treatment to induce crystallization. However, the high-temperature post-treatment and long-period heating may result in phase separation of the dopant metal ions as respective metal oxides. Such metal oxides can act as an electron–hole recombination center, resulting in the decrease of photocatalytic activity [22]. For the impregnation method, the substitution of metal ions for oxygen is unlikely to occur in bulk TiO_2 crystallites, perhaps only on the surface [23]. In the case of liquid phase deposition, a very long aging time is often unavoidable for obtaining a certain amount of sample. Ion-implantation method has the disadvantage of using complicated and expensive facilities.

In contrast to wet methods that need multiple processing steps and long processing times, flame synthesis, especially flame spray pyrolysis (FSP), is a versatile one-step process for synthesizing a variety of nanoparticles [24–26]. In this process, chemical reactions of precursor compounds are driven by a flame, resulting in the formation of clusters, which further grow to nanometer-sized particles by coagulation and sintering [25]. It has been reported that materials prepared by FSP often exhibit high surface area and thermal stability [27–29], both of which are desirable properties for the design of heterogeneous catalysts. In recent years, FSP has been

* Corresponding author. Tel.: +86 21 64250949; fax: +86 21 64250624.
E-mail address: czli@ecust.edu.cn (C. Li).

1385-8947/$ – see front matter © 2009 Elsevier B.V. All rights reserved.
doi:10.1016/j.cej.2009.02.030

used for the synthesis of photocatalysts such as TiO_2 [30], Pt–TiO_2 [31], Ag–ZnO [32], Fe–TiO_2 [33], MoO_3/TiO_2 [34], which often show excellent photocatalytic activity compared with the photocatalysts synthesized by other methods. Lately, FSP was also used to prepare V_2O_5/TiO_2 (V_2O_5 supported on TiO_2 surface) catalyst, which exhibit high catalytic activity for o-xylene oxidation [35]. However, to the best of knowledge, the study involving photocatalytic activity of V-doped TiO_2 nanoparticles prepared by FSP has never been reported.

In the present study, the one-step flame spray pyrolysis technique was used to prepare V-doped TiO_2 nanoparticles. The structural and optical properties of the obtained samples were characterized by XRD, TEM, EPR, UV–vis absorption spectroscopy, and nitrogen adsorption–desorption methods. The photocatalytic activities of V–TiO_2 samples under UV and visible light irradiation were evaluated by measuring the concentration changes of methylene blue (MB) and 2,4-dichlorophenol (2,4-DCP), respectively. The photocatalytic mechanisms for V–TiO_2 samples under UV and visible light irradiation were tentatively discussed.

2. Experimental

2.1. Flame synthesis of V–TiO_2 catalysts

V–TiO_2 nanoparticles were synthesized using a spray flame setup consisting of an atomization nozzle surrounded by a flamelet ring (Fig. 1). Precursor solutions were beforehand prepared by dissolving appropriate amounts of titanium tetrabutoxide ($Ti(OC_4H_9\text{-}n)_4$, 98%, Lingfeng Chemical reagent Co., Ltd., China) and vanadium diacetylacetone ($VO(AcAc)_2$, 99%, Jincang Reagent Co., China) in anhydrous ethanol (C_2H_5OH, 99.7%, Sinopharm Chemical Reagent Co. Ltd., China). The concentration of titanium was always 0.5 M, while the V concentration was chosen as 0.25, 0.5, 1.0, 2.0, 3.0 and 5.0, which was the mole percentage of V in the theoretical TiO_2 powder. Using a syringe pump, the precursor solution was delivered to the atomization nozzle (2.5 mL/min), where it was dispersed into fine droplets by O_2 (4.5 L/min). The pressure drop at the nozzle tip was maintained at 1.2 bar. The liquid spray was ignited by a circular flame of methane (1.0 L/min) and oxygen (2.4 L/min) around the nozzle outlet. Additional oxygen (5 L/min) was provided through the outermost sintered metal ring as sheath for the supported flame. The visual height of the main flame under above-mentioned condition was about 6 cm. A Pt–Rh thermocouple was used to measure the flame temperature in the absence of titanium and vanadium precursor to avoid particle deposition on the thermocouple. The flame temperatures at 2, 3.5, and 5 cm above the nozzle were 1800, 1200, and 800 K, respectively. The flame temperature near to the nozzle was not measured to avoid the break of thermocouple. The synthesized nanoparticles were deposited on the inner surface of a cylindrical stainless tank and exhaust gases were extracted using a pump. The obtained samples are designated as *x*%V–TiO_2, where *x* is the mole percentage of V in the theoretical TiO_2 powder. The production yields for different V–TiO_2 samples are near to 80%.

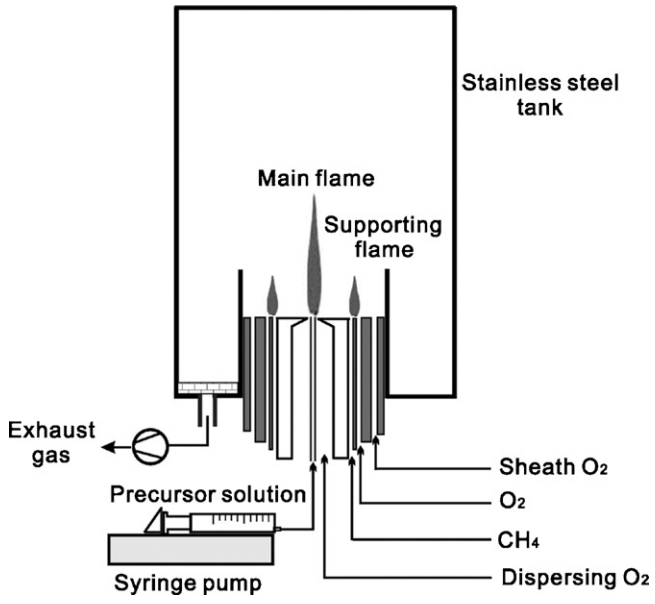

Fig. 1. Schematic diagram of flame spray pyrolysis apparatus for preparing V–TiO_2 catalysts. The precursor solution is rapidly dispersed by an oxygen stream and ignited by a methane/oxygen supporting flame.

To compare the influence of preparation method on the photocatalytic activity of V–TiO_2 catalysts, V–TiO_2 samples were also prepared by a modified sol–gel method [19]. $VO(AcAc)_2$ was dissolved in the anhydrous ethanol, while $Ti(OC_4H_9\text{-}n)_4$ was dissolved in the mixture of acetic acid and anhydrous ethanol. The molar ratio of Ti and acetic acid was 1:6. Under continuous stirring, the above two solutions were mixed and hydrolysis reaction was driven by the water generated via the esterification of acetic acid and ethanol. After being stirred for 24 h, the mixture was dried at 150 °C and pulverized to powder. Finally, the obtained powder was calcined at 673 K for 1 h, designated as *x*%V–TiO_2-S.

2.2. Characterization

The phases and crystallite sizes of the prepared samples were characterized by X-ray diffraction (XRD), performed on a Rigaku D/max 2550 VB/PC X-ray diffractometer at room temperature. The patterns were recorded over the angular range 15–75° (2θ), using Cu Kα radiation ($\lambda = 0.154056$ nm) with working voltage and current of 40 kV and 100 mA, respectively. Transmission electron microscopy (TEM) measurements were performed on a Hitachi H-800 transmission electron microscopy, operated at an acceleration voltage of 200 kV. The UV–vis absorption spectra of V–TiO_2 samples were obtained using a Scan UV–vis–NIR spectrophotometer (Varian Cary 500) equipped with an integrating sphere assembly, using polytetrafluoroethylence as a reference material. The X-band electron paramagnetic resonance (EPR) spectra were recorded at 100 K using a Bruker EMX-8/2.7 EPR spectrometer. The Brunauer–Emmett–Teller (BET) specific surface area (S_{BET}) of the samples were determined by using nitrogen adsorption in a Micromeritics ASAP 2010 nitrogen-adsorption apparatus. All the samples were degassed at 473 K prior to the measurements.

2.3. Photocatalytic activity measurement

Methylene blue and 2,4-dichlorophenol were selected as target pollutants to evaluate the photocatalytic activities of V–TiO_2 samples under UV and visible light irradiation, respectively. Photodegradation reactions were carried out using a home-made setup, for which a lamp was cooled with flowing water in a quartz cylindrical jacket around the lamp, and a fanner was fixed for maintaining a constant temperature during the photocatalytic reaction. A 300-W high-pressure Hg lamp and a 1000-W tungsten halogen lamp equipped with a UV cut-off filters ($\lambda > 420$ nm) were used as UV and visible light sources, respectively. For each test, 0.05 g of catalyst sample was added into an quartz tube containing 50 mL of 20 mg/L MB (or 100 mg/L 2,4-DCP) aqueous solution. Prior to light irradiation, the suspensions were sonicated for 10 min and stirred for 30 min in dark to attain the adsorption–desorption equilibrium for model pollutant and dissolved oxygen on the surface of TiO_2. At given time interval, about 4 mL suspension was withdrawn, centrifugated and filtered to remove the remained particles. The

concentrations of MB (or 2,4-DCP) before and after light irradiation were determined with a UV–vis spectrophotometer, and the degradation rates of MB (or 2,4-DCP) at different time intervals were calculated according to the determined absorbance values.

3. Results and discussion

3.1. Structural and textural properties of V–TiO_2 catalysts

It is well known that metal doping can sometimes change the crystal structure, particle size, morphology and specific surface area of TiO_2, all of which are important factors that determine the photocatalytic activity of TiO_2. Furthermore, the final photocatalytic activity of metal-doped TiO_2 is also relative to the existence states of metal dopant (in the matrix or on surface of TiO_2, chemical state, and so on), which not only influence the transfers of photo-induced electrons and holes but also change the light absorption properties of TiO_2. Therefore, the structural and textural properties of V–TiO_2 catalysts were characterized by XRD, TEM, EPR, and nitrogen adsorption–desorption methods.

Fig. 2 shows the XRD patterns of undoped TiO_2 and different V–TiO_2 samples. As shown in Fig. 2(a–f), all samples mainly consist of anatase (JCPDS, No. 21-1272) together with minor rutile (JCPDS No. 21-1276). No characteristic peak attributed to vanadium oxides (V_2O_5 or V_2O_4) were found in the XRD patterns, implying that either V was incorporated into the crystal lattice of TiO_2, or vanadium oxide is very small and homogeneously dispersed [19]. Schimmoeller et al. [35] reported that weak reflections corresponding crystalline VO_2 can be found when V_2O_5 content is higher than 7 wt.% (6.1 at.%). Since the V contents for all V–TiO_2 samples in this study are below 5 at.%, it is reasonable that no characteristic peak attributed to vanadium oxides was found in the XRD patterns.

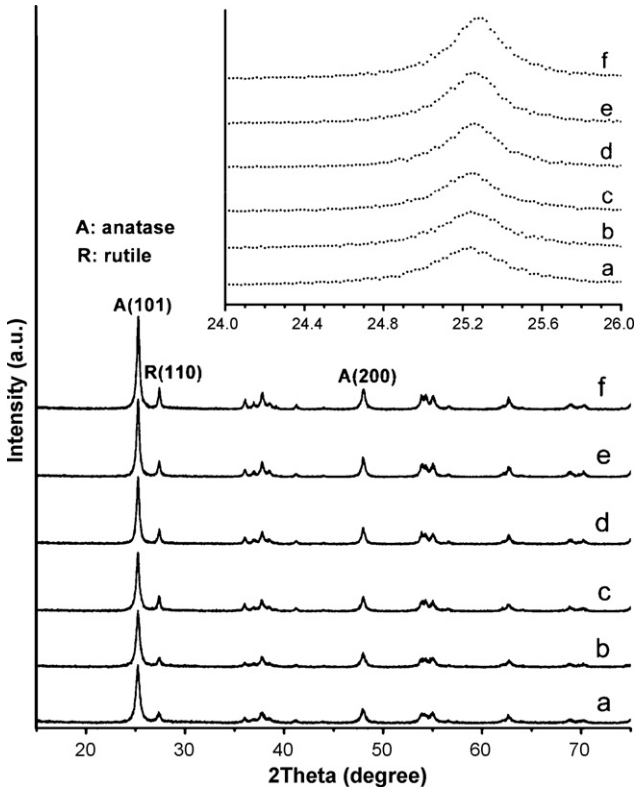

Fig. 2. XRD patterns of (a) undoped TiO_2, (b) 0.25%V–TiO_2, (c) 0.5%V–TiO_2, (d) 1%V–TiO_2, (c) 3%V–TiO_2, and 5%V–TiO_2. The inset is an enlargement of the anatase (1 0 1) peaks for these samples.

Table 1
Physicochemical properties of undoped TiO_2 and V–TiO_2 samples.

Sample	Phase, content[a] (nm) and crystallite size[b]		S_{BET} (m^2/g)	d_{BET}[c] (nm)
	Anatase	Rutile		
Undoped TiO_2	89.5% (13.9)	10.5% (18.5)	98.1	15.9
0.25%V–TiO_2	89.2% (16.4)	10.8% (26.3)	79.3	19.7
0.50%V–TiO_2	88.4% (17.3)	11.6% (26.1)	74.1	21.1
1%V–TiO_2	88.2% (18.4)	11.8% (27.3)	66.7	23.4
3%V–TiO_2	87.6% (20.3)	12.4% (27.7)	63.2	24.7
5%V–TiO_2	86.6% (20.9)	13.4% (29.6)	57.8	27

[a] Determined by XRD using Eq. (1).
[b] Calculated by Debye–Scherrer formula.
[c] Calculated by Eq. (3).

The inset of Fig. 2 is an enlargement of the anatase (1 0 1) peaks for these samples. A slight shift of anatase (1 0 1) peak was found after V doping (e.g., $2\theta = 25.22^\circ$ for undoped TiO_2, 25.24° for 1%V–TiO_2, 25.28° for 5%V–TiO_2), indicating the decrease of lattice parameters and the occurrence of lattice distortion in the anatase structure. The shrinkage of unit cell is due to the incorporation of V^{4+}, whose radius (0.72 Å) is smaller than that of Ti^{4+} (0.74 Å) [36]. The phase contents of anatase and rutile in the samples were calculated from the respective peak intensities of anatase (1 0 1) and rutile (1 1 0) with the following equation [37]:

$$W_R = \frac{A_R}{0.884A_A + A_R} \quad (1)$$

where W_R represents the weight fraction of rutile. A_A and A_R are the integrated intensities of anatase (1 0 1) and rutile (1 1 0) peaks, respectively. As shown in Table 1, the content of rutile slightly increases with increasing V doping, which is consistent with the results reported by other investigators [21,38]. This phenomenon might be relative to the lattice distortion caused by the substitution of the Ti site by V ions, which can decrease the thermal stability of anatase and favor the phase transition from anatase to rutile. It is well known that rutile is more thermodynamically stable than anatase. In addition, the ionic radius of V^{4+} is slightly smaller than that of Ti^{4+}. Therefore, the shrinkage of the unit cell of V–TiO_2 is expected to favor the formation of more compactly packed rutile ($\rho_{rutile} = 4.26\,g/cm^3$, $\rho_{anatase} = 3.84\,g/cm^3$) [39]. The average crystallite sizes of anatase and rutile in the samples were calculated by applying the Debye–Scherrer formula (Eq. (2)) on the anatase (1 0 1), and rutile (1 1 0) diffraction peaks and were listed in Table 1:

$$D = \frac{K\lambda}{\beta\cos\theta} \quad (2)$$

where D is the average crystallite size, K is a constant which is taken as 0.89 here, λ is the wavelength of the X-ray radiation (Cu Kα = 0.154056 nm), β is the corrected band broadening (full width at half-maximum (fwhm)) after subtraction of equipment broadening, and θ is the diffraction angle. As shown in Table 1, the crystalline size of anatase TiO_2 increases with increasing V concentration, similar to the results reported by other investigators [18,19]. Assuming that all particles are ideally monodisperse spheres, the average BET-equivalent particle diameter (d_{BET}) can be calculated by using the following equation:

$$d_{BET} = \frac{6}{S_{BET}\rho_{TiO_2}} \quad (3)$$

where ρ_{TiO_2} is the density of anatase TiO_2 ($3.84\,g/cm^3$). As shown in Table 1, for each sample the average primary particle size (d_{BET}) is slightly larger than the corresponding average crystallite size of anatase and smaller than that of rutile. Two reasons might be responsible for this phenomenon. One is because all samples con-

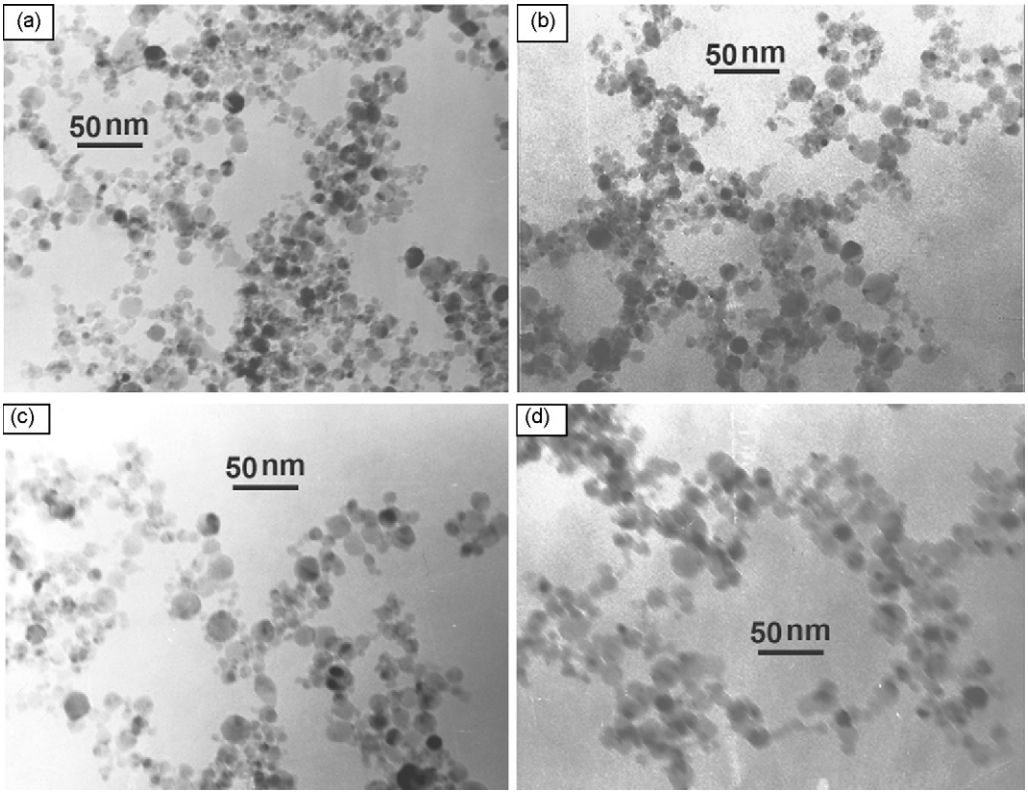

Fig. 3. TEM images of (a) undoped TiO_2, (b) 0.5%V–TiO_2, (c) 1%V–TiO_2, and (d) 5%V–TiO_2.

sist of anatase and rutile (Table 1), the other is probably related to the agglomeration of monocrystalline primary particles.

Fig. 3 shows the TEM images of undoped TiO_2, 0.5%V–TiO_2, 1%V–TiO_2, and 5%V–TiO_2. It was found that all the samples consist of spherical nanoparticles with broad size distribution (e.g., 5–25 nm for undoped TiO_2, 8–30 nm for 5%V–TiO_2). The nanoparticles synthesized by FSP technique often exhibit spherical morphology and broad size distribution [33,35]. In FSP process, product particles are formed by droplet evaporation, combustion, aerosol formation, coagulation, and sintering [27,40,41]. In the flame, product vapor condenses into small particles, which can further form bigger particles by colliding and coalescing with each other. It is obvious that increasing the residence time of product particles in the fame favors the increase of primary particle size. Compared with smaller spray droplets, larger spray droplets evaporate more slowly and have longer residence time in the flame, leading to prolonged particle formation. Therefore, the particles derived from small spray droplets exhibit longer residence time in the flame than those derived from large spray droplets. As a result, small spray droplets favor the increase of primary particle size, while, large spray droplets favor the decrease of primary particle size. To a great extent, the broad size distribution of the obtained nanoparticles (Fig. 3) results from the variation of spray droplets in size. In addition, the reason that nanoparticles formed in flame spray show spherical is due to high surface tension, which was discussed by Miquel et al. [42].

As a highly sensitive technique for examining paramagnetic species and the lattice information, EPR spectroscopy was used to investigate the V-doped TiO_2 samples. Fig. 4 shows the EPR spectra of 0.25%V–TiO_2, 0.5%V–TiO_2, 1%V–TiO_2, and 3%V–TiO_2. It was found 0.5%V–TiO_2, 1%V–TiO_2, and 3%V–TiO_2 exhibit obvious eight-component hyperfine structure, indicating that V^{4+} ions have been incorporated into the crystal lattice of TiO_2 in the form of substitutional V [43,44]. The paramagnetic V^{4+} ion has the 3d electronic configuration and an electronic spin $S = 1/2$. The nuclear spin for the ^{51}V isotope is $I = 7/2$. Therefore, the eightfold hyperfine structure can be attributed to the dipole–dipole interaction between the magnetic moment of the ^{51}V nucleus and the electronic moment of the paramagnetic V^{4+} ions. In the case of sample 0.25%V–TiO_2, the eightfold hyperfine structure cannot be clearly identified due to the low signal intensity. Compared with V^{5+} ion (0.068 nm), the ion radius of six-coordinated V^{4+} (0.072 nm) is much closer to that of Ti^{4+} (0.074 nm) [36], implying that V^{4+} ions are easier to substitute Ti^{4+} in TiO_2 lattice than V^{5+} ions. V dopants in TiO_2 have

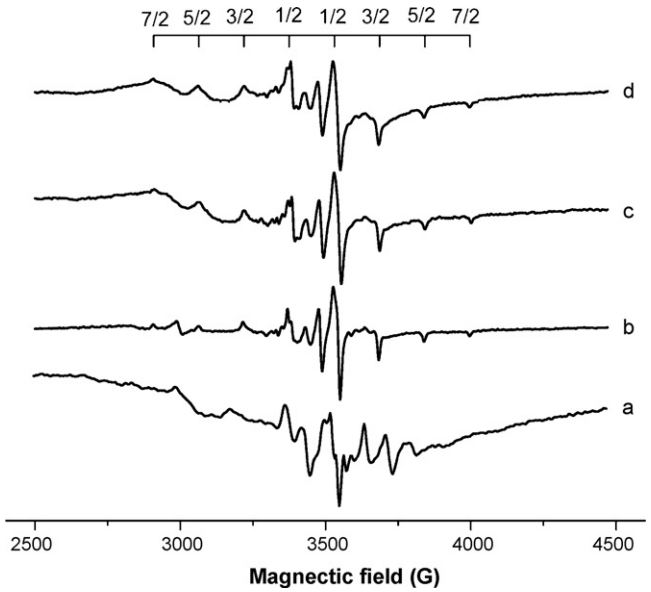

Fig. 4. EPR spectra at 100 K of (a) 0.5%V–TiO_2, (b) 1%V–TiO_2, and (c) 3%V–TiO_2.

been determined to preferentially substitute for Ti^{4+}, rather than to access interstitial sites [45]. Furthermore, Some studies have proved the formation of solid solubility between TiO_2 and VO_2 [36,44]. In our experiment, short residence time coupled with high quenching rate during the flame synthesis perhaps prevents phase segregation once V is incorporated into TiO_2 lattice. It has been mentioned that the signal intensity of eight-component hyperfine structure is proportional to the intralattice V amount [43,44]. From 1%V–TiO_2 to 3%V–TiO_2, only a slight increase of the signal intensities was found, implying that not all V ions can be incorporated into the crystal lattice of TiO_2 as substitutional V^{4+} when V concentration is too high. Recently, a theoretical study indicated that V^{4+} could be stabilized into TiO_2 structure while V^{5+} is likely the major chemical state at the surface of the material [46]. It also has been reported that the isolated mono-oxo vanadyl centers exist on the surface of TiO_2 at low cover [47,48]. So, part V in sample 3%V–TiO_2 might be present in the form of pentavalent V, which does not give ESR signals. Some investigators found that coverages of at least three supported monolayers of TiO_2 are necessary before resolved XRD spectra are obtained [49]. So, it may be reasonable to think that vanadium oxides also cannot be detected by XRD when it comprised of only one or two monolayers.

3.2. Light absorption properties

As mentioned above, doping with transition metals can extend the light absorption of TiO_2 into the visible region, resulting in the enhancement of visible light photocatalytic activity. Fig. 5 shows the UV–vis absorption spectra of undoped TiO_2 and different V–TiO_2 samples. As shown in Fig. 5, the absorption edge of undoped TiO_2 emerges at 394 nm, corresponding to the band-gap energy of 3.14 eV. This value is slightly smaller than the reported value of anatase (E_g = 3.2–3.3 eV) [50], ascribed to the presence of minor rutile (E_g = 3.0 eV) in the sample. Compared with the undoped TiO_2, all of the V–TiO_2 samples exhibit a red-shift of absorption edge and a significant enhancement of light absorption in the visible light region. Both of red-shift of absorption edge and light absorption in the visible light region increase with increasing the V concentration. It has been reported that the red-shift of absorption edge is attributed to the charge-transfer transition between the d electrons of the dopant and the conduction band (or valence band) of TiO_2 [7]. In the case of V–TiO_2, the red-shift of absorption edge should be attributed to the electron transition from the VB (O 2p) to the t_{2g} level of V 3d orbit because V 3d orbit is located at the bottom of the conduction band of TiO_2. It has been pointed that some metal cations presented in adequate oxidation state can additionally introduce detectable d–d transitions in the UV–vis spectra [51]. So, the light absorption in visible region is partly attributed to the d–d transition of V, similar to that of Fe [52].

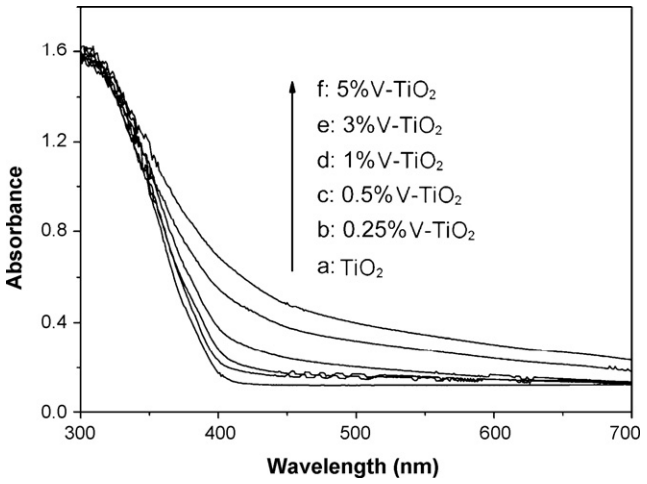

Fig. 5. UV–vis absorption spectra of (a) undoped TiO_2, (b) 0.25%V–TiO_2, (c) 0.5%V–TiO_2, (d) 1%V–TiO_2, (e) 3%V–TiO_2, and (f) 5%V–TiO_2.

3.3. Photocatalytic activity and mechanism analysis

Fig. 6A shows the degradation curves of MB over different V–TiO_2 samples as a function of UV light irradiation time. In Fig. 6A, C_0 is the concentration of MB after adsorption–desorption equilibrium, while C represents MB concentration at certain time interval. It was found that the optimal V concentration for attaining the highest photocalytic activity is 0.5%. When the V concentration is below this level, the photocatalytic activity of V–TiO_2 slightly increases

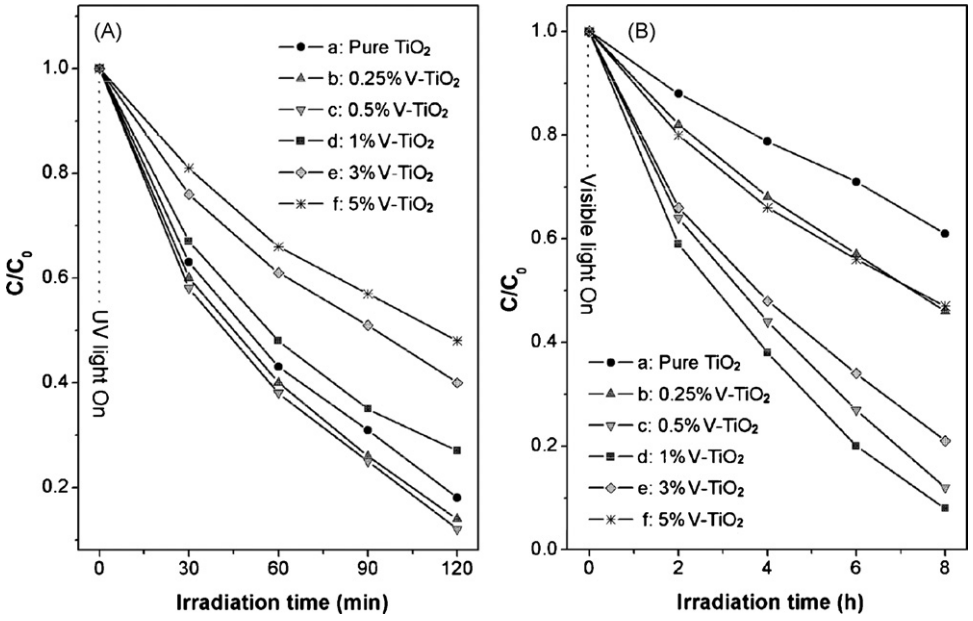

Fig. 6. Concentration changes of (A) MB as a function of UV-irradiation time (min) and (B) 2,4-DCP as a function of visible light irradiation time (h) over different V–TiO_2 samples: (a) undoped TiO_2, (b) 0.25%V–TiO_2, (c) 0.5%V–TiO_2, (d) 1%V–TiO_2, (e) 3%V–TiO_2, and (f) 5%V–TiO_2.

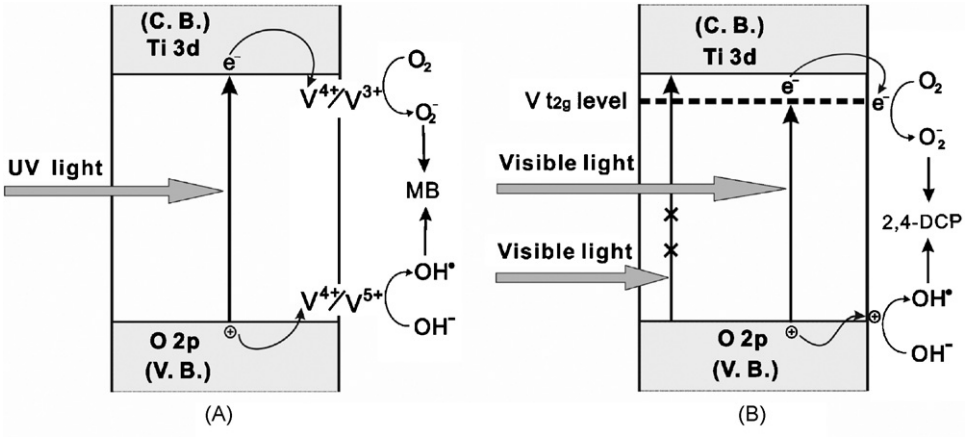

Fig. 7. Schematic diagram to illustrate the mechanism of V doping: (A) photocatalytic degradation of MB under UV light irradiation and (B) photocatalytic degradation of 2,4-DCP under visible light irradiation.

with the increase of V concentration. However, the photocatalytic activity of V–TiO_2 rapidly decreases with the increase of V concentration when the V doping is more than 0.5%. It is well known that both of the crystalline structure and specific surface area are two important factors that influence the photocatalytic activity of TiO_2. However, in this study, only little variation of crystalline structure was found for different V–TiO_2 samples. Although the specific surface area decreases with the increase of V concentration, the variation of photocatalytic activity is not consistent with the variation of specific surface area. So, the variation of photocatalytic activity of different V–TiO_2 samples cannot be mainly assigned to the influences of crystalline structure and specific surface area. It has been reported that metal dopants can influence the photocatalytic activity of TiO_2 by acting as electron (or hole) traps and by altering the recombination rate of electron/hole pairs [7]. On the basis of this theory and the above experimental results, the photocatalytic degradation processes were proposed and elucidated in Fig. 7A and Eqs. (4)–(9). Because the energy level for V^{4+}/V^{3+} lies below the conduction band edge of TiO_2 and the energy level for V^{4+}/V^{5+} lies above the valence band edge [7], V^{4+} ions, acting as both electron and hole traps, can turn into V^{3+} and V^{5+} ions by trapping photogenerated electrons and holes, respectively (Eqs. (4) and (5)). Subsequently, the trapped electrons and holes are released (Eqs. (6) and (7)) and migrate to the surface of TiO_2. By accepting an electron, the adsorbed O_2 on the surface of TiO_2 is reduced to O_2^- (Eq. (8)), while surface hydroxyl group translates into hydroxyl radical ($OH^\bullet$) by accepting a hole (Eq. (9)). Both of O_2^- and $OH^\bullet$ can further degrade MB. As a result, the introduction of appropriate amount of V^{4+} ions in TiO_2 lattice can restrain the recombination rate of photogenerated electrons and holes, enhancing the photocatalytic activity of TiO_2. However, when the concentration of V^{4+} ions is too high, V^{4+} ions can act as the recombination centers of photogenerated electrons and holes, resulting in the decrease of photocatalytic activity. In this study, the optimal V concentration is 0.5%. Above this level, V^{4+} ions steadily become the recombination centers of photogenerated electrons and holes, evidently decreasing the photocatalytic activity of TiO_2:

$$V^{4+} + e^- \rightarrow V^{3+} \quad (4)$$

$$V^{4+} + h^+ \rightarrow V^{5+} \quad (5)$$

$$V^{3+} \rightarrow V^{4+} + e^- \quad (6)$$

$$V^{5+} \rightarrow V^{4+} + h^+ \quad (7)$$

$$V^{3+} + O_2\,(ads) \rightarrow V^{4+} + O_2^- \quad (8)$$

$$V^{5+} + OH^-\,(ads) \rightarrow V^{4+} + {}^\bullet OH\,(ads) \quad (9)$$

Dyes can be degraded under visible light irradiation via two competitive processes: a photocatalytic process and a self-photosensitized process. Thus, it is very difficult to tell apart the two processes when dyes were employed, which is unfavorable for the study of degradation mechanism. Here, we selected 2,4-dichlorophenol which has no absorption in the visible region as target pollutant to evaluate the photocatalytic activity of V–TiO_2 under visible light irradiation. Fig. 6B shows the degradation curves of 2,4-DCP over different V–TiO_2 samples as a function of visible light irradiation time. It was found that the photocatalytic activity of the V–TiO_2 samples increases with increasing V concentration at the beginning, and then has downtrend with further increasing V concentration. Under visible light irradiation, the optimal doping level of V^{4+} ions is 1%. It is noteworthy that V doping enhances the photocatalytic activity more evidently under visible light irradiation compared to that under UV light irradiation. For instance, under UV light irradiation for 1 h, the optimal degradation rate of MB over 0.5%V–TiO_2 is only 8% higher than that over undoped TiO_2, while under visible light irradiation for 4 h, the degradation rate of 2,4-DCP over 1%V–TiO_2 is two times higher than that over undoped TiO_2. This result implies that the photoactive enhancement mechanisms under UV and visible light irradiation are different. As illustrated in Fig. 7B, the excitation behavior of V–TiO_2 under visible irradiation might be related to V 3d orbital. Due to the fact that the t_{2g} level of V 3d orbital lies a little below the conduction band edge of TiO_2 [51], electrons can be excited form the valence band of TiO_2 to the t_{2g} level of V 3d orbital under visible light irradiation, and further migrate to adsorbed O_2 to form O_2^-. Meanwhile, holes migrate to surface hydroxyl group to produce hydroxyl radicals ($^\bullet OH$). Thus, 2,4-DCP was degraded under visible light irradiation. Although red-shift of absorption edge and light absorption in the visible light region increase with increasing the V concentration, it does not mean that the photocatalytic activity under visible light irradiation always increases with the increase of V concentration. On the contrary, too high V concentration can lead to the decrease of photocatalytic activity. This phenomenon might be related to several reasons. Firstly, when the concentration of V^{4+} ions is too high, they can become the recombination centers of photogenerated electrons and holes, similar to that under UV light irradiation. Secondly, the specific surface area decreases with the increase of V concentration, while low specific surface area is always unfavorable for obtaining high photocatalytic activity. Finally, excess V dopant might form low cover on the TiO_2 surface, which not only influences the penetration of light but also reduces

the contact area between TiO_2 and organic pollutant. As a result, excess V concentration leads to the decrease of photocatalytic activity.

The photocatalytic activities of V–TiO_2 catalysts prepared by sol–gel method were also measured. It was found that V–TiO_2 catalysts prepared by FSP exhibit evidently higher photocatalytic activity than the samples prepared by sol–gel method under both UV and visible light irradiation. For instance, under visible light irradiation for 4 h, the optimal degradation rates of 2,4-DCP over FSP-made V–TiO_2 (1%V–TiO_2) and sol–gel-made V–TiO_2 (2%V–TiO_2-S) were 62% and 45%, respectively. Further study is currently under way to elucidate the effect of preparation method on photocatalytic activity.

4. Conclusions

By a simple one-step flame spray pyrolysis technique, V–TiO_2 nanoparticles have been synthesized successfully. It reveals that all V–TiO_2 samples consist of anatase and rutile, and V doping favors the primary particle size growth together with the increase of rutile content. Benefiting from the short residence time and high quenching rate during the flame spray process, V dopant has been successfully incorporated into the crystal lattice of TiO_2 in the form of V^{4+} ion. Although V doping can enhance the photocatalytic activity under both UV and visible light irradiation, the improvement of photocatalytic activity under visible light irradiation is more evident than that under UV light irradiation, e.g., under UV light irradiation for 1 h, the optimal degradation rate of MB over 0.5%V–TiO_2 is only 8% higher than that over undoped TiO_2, while under visible light irradiation for 4 h, the degradation rate of 2,4-DCP over 1%V–TiO_2 is two times higher than that over undoped TiO_2. Under UV light irradiation, appropriate amount of V doping can decrease the recombination of photogenerated electrons and holes, resulting in the enhancement of photocatalytic activity. Due to the excitation of electrons from the valence band of O 2p to the 3d orbit of V, V doping can shift the light absorption of TiO_2 into the visible light region, resulting in the evident enhancement of photocatalytic activity under visible light irradiation. In summary, flame spray pyrolysis is promising technique for the preparation of metal-doped TiO_2 photocatalysts with high visible light photocatalytic activity.

Acknowledgements

This work has been supported by the National High Technology Research and Development Program of China (2006AA03Z358), the National Natural Science Foundation of China (20706015, 50703009), the Shanghai Rising-Star Program (06QA14013, 07QA14014), the Major Basic Research Project of Shanghai (07DJ14001), the Ph.D. Programs Foundation of Ministry of Education of China (20070251022), the Special Projects for Key Laboratories in Shanghai (07DZ22016, 06DZ22008), the Special Projects for Nanotechnology of Shanghai (0752nm010, 0652nm034).

References

[1] J.C. Zhao, T.X. Wu, K.Q. Wu, K. Oikawa, H. Hidaka, N. Serpone, Photoassisted degradation of dye pollutants (III) degradation of the cationic dye rhodamine B in aqueous anionic surfactant/TiO_2 dispersions under visible light irradiation: evidence for the need of substrate adsorption on TiO_2 particles, Environ. Sci. Technol. 32 (1998) 2394–2400.
[2] A. Fujishima, T.N. Rao, D.A. Truk, Titanium dioxide photocatalysis, J. Photochem. Photobiol. C 1 (2000) 1–21.
[3] J.C. Yu, W. Ho, J. Yu, H. Yip, P.K. Wong, J. Zhao, Efficient visible-light-induced photocatalytic disinfection on sulfur-doped nanocrystalline titania, Environ. Sci. Technol. 39 (2005) 1175–1179.
[4] M.R. Hoffmann, S.T. Martin, W. Choi, D.W. Bahnemann, Environmental applications of semiconductor photocatalysis, Chem. Rev. 95 (1995) 69–96.
[5] T. Wu, G. Liu, J. Zhao, H. Hidaka, N. Serpone, Evidence for H_2O_2 generation during the TiO_2-assisted photodegradation of dyes in aqueous dispersions under visible light illumination, J. Phys. Chem. B 103 (1999) 4862–4867.
[6] W. Zhao, C.C. Chen, X.Z. Li, J.C. Zhao, H. Hidaka, N. Serpone, Photodegradation of sulforhodamine-B dye in platinized titania dispersions under visible light irradiation: influence of platinum as a functional co-catalyst, J. Phys. Chem. B 106 (2002) 5022–5028.
[7] W. Choi, A. Termin, M.R. Hoffmann, The role of metal ion dopants in quantum-sized TiO_2: correlation between photoreactivity and charge carrier recombination dynamics, J. Phys. Chem. 98 (1994) 13669–13679.
[8] A. Di Paola, G. Marci, L. Palmisano, M. Schiavello, K. Uosaki, S. Ikeda, B. Ohtani, Preparation of polycrystalline TiO_2 photocatalysts impregnated with various transition metal ions: characterization and photocatalytic activity for the degradation of 4-nitrophenol, J. Phys. Chem. B. 106 (2002) 637–645.
[9] J.F. Zhu, W. Zheng, B. He, J.L. Zhang, M. Anpo, Characterization of Fe–TiO_2 photocatalysts synthesized by hydrothermal method and their photocatalytic reactivity for photodegradation of XRG dye diluted in water, J. Mol. Catal. A 216 (2004) 35–43.
[10] J.F. Zhu, Z.G. Deng, F. Chen, J.L. Zhang, H.J. Chen, M. Anpo, J.Z. Huang, L.Z. Zhang, Hydrothermal doping method for preparation of Cr^{3+}–TiO_2 photocatalysts with concentration gradient distribution of Cr^{3+}, Appl. Catal. B 62 (2006) 329–335.
[11] M. Anpo, S. Dohshi, M. Kitano, Y. Hu, M. Takeuchi, M. Matsuoka, The preparation and characterization of highly efficient titanium oxide-based photofunctional materials, Annu. Rev. Mater. Res. 35 (2005) 1–27.
[12] M. Anpo, M. Takeuchi, The design and development of highly reactive titanium oxide photocatalysts operating under visible light irradiation, J. Catal. 216 (2003) 505–516.
[13] H. Yamashita, M. Anpo, Application of an ion beam technique for the design of visible light-sensitive, highly efficient and highly selective photocatalysts: ion-implantation and ionized cluster beam methods, Catal. Surv. Asia 8 (2004) 35–45.
[14] H. Yamashita, M. Harada, J. Misaka, M. Takeuchi, K. Ikeue, M. Anpo, Degradation of propanol diluted in water under visible light irradiation using metal ion-implanted titanium dioxide photocatalysts, J. Photochem. Photobiol. A 148 (2002) 257–261.
[15] J.K. Zhou, M. Takeuchi, X.S. Zhao, A.K. Ray, M. Anpo, Photocatalytic decomposition of formic acid under visible light irradiation over V-ion-implanted TiO_2 thin film photocatalysts prepared on quartz substrate by ionized cluster beam (ICB) deposition method, Catal. Lett. 106 (2006) 67–70.
[16] J.C. Yu, J. Lin, R.W.M. Kwok, Enhanced photocatalytic activity of $Ti_{1-x}V_xO_2$ solid solution on the degradation of acetone, J. Photochem. Photobiol. A 111 (1997) 199–203.
[17] S. Klosek, D. Raftry, Visible light driven V-doped TiO_2 photocatalyst and its photooxidation of ethanol, J. Phys. Chem. B 105 (2001) 2815–2819.
[18] D.E. Gu, B.C. Yang, Y.D. Hu, A novel method for preparing V-doped titanium dioxide thin film photocatalysts with high photocatalytic activity under visible light irradiation, Catal. Lett. 118 (2007) 254–259.
[19] Jeffrey C.-S. Wu, Chih-Hsien Chen, A visible-light response vanadium-doped titania nanocatalyst by sol–gel method, J. Photochem. Photobiol. A 163 (2004) 509–515.
[20] L.E. Briand, R.D. Bonetto, M.A. Sanchez, H.J. Thomas, Structural modelling of coprecipitated VTiO catalysts, Catal. Today 32 (1996) 205–213.
[21] S.T. Martin, C.L. Morrison, M.R. Hoffmann, Photochemical mechanism of size-quantized vanadium-doped TiO_2 particles, J. Phys. Chem. 98 (1994) 13695–13704.
[22] K.E. Karakitsou, X.E. Verykios, Effects of altervalent cation doping of titania on its performance as a photocatalyst for water cleavage, J. Phys. Chem. 97 (1993) 1184–1189.
[23] B. Grzybowska, J. Słoczyński, R. Grabowski, K. Samson, I. Gressel, K. Wcisło, L. Gengembre, Y. Barbaux, Effect of doping of TiO_2 support with altervalent ions on physicochemical and catalytic properties in oxidative dehydrogenation of propane of vanadia–titania catalysts, Appl. Catal. A 230 (2002) 1–10.
[24] H.K. Kammler, L. Mädler, S.E. Pratsinis, Flame synthesis of nanoparticles, Chem. Eng. Technol. 24 (2001) 583–596.
[25] S.E. Pratsinis, Flame aerosol synthesis of ceramic powders, Prog. Energ. Combust. Sci. 24 (1998) 197–219.
[26] M.S. Wooldridge, Gas-phase combustion synthesis of particles, Prog. Energ. Combust. Sci. 24 (1998) 63–87.
[27] R. Strobel, F. Krumeich, W.J. Stark, S.E. Pratsinis, Flame spray synthesis of Pd/Al_2O_3 catalysts and their behavior in enantioselective hydrogenation, J. Catal. 222 (2004) 307–314.
[28] W.J. Stark, M. Maciejewski, L. Mädler, S.E. Pratsinis, A. Baiker, Flame-made nanocrystalline ceria/zirconia: structural properties and dynamic oxygen exchange capacity, J. Catal. 220 (2003) 35–43.
[29] W.J. Stark, J.-D. Grunwaldt, M. Maciejewski, S.E. Pratsinis, A. Baiker, Flame-made Pt/ceria/zirconia for low-temperature oxygen exchange, Chem. Mater. 17 (2005) 3352–3358.
[30] W.Y. Teoh, F. Denny, R. Amal, D. Friedmann, L. Mädler, S.E. Pratsinis, Photocatalytic mineralisation of organic compounds: a comparison of flame-made TiO_2 catalysts, Top. Catal. 44 (2007) 489–497.
[31] W.Y. Teoh, L. Mädler, D. Beydoun, S.E. Pratsinis, R. Amal, Direct (one-step) synthesis of TiO_2 and Pt/TiO_2 nanoparticles for photocatalytic mineralisation of sucrose, Chem. Eng. Sci. 60 (2005) 5852–5861.
[32] M.J. Height, S.E. Pratsinis, O. Mekasuwandumrong, P. Praserthdam, Ag–ZnO catalysts for UV-photodegradation of methylene blue, Appl. Catal. B 63 (2006) 305–312.

[33] W.Y. Teoh, R. Amal, L. Mädler, S.E. Pratsinis, Flame sprayed visible light-active Fe–TiO_2 for photomineralisation of oxalic acid, Catal. Today 120 (2007) 203–213.
[34] W. Lee, Y.R. Do, K. Dwight, A. Wold, Enhancement of photocatalytic activity of titanium(IV) oxide with molybdenum(VI) oxide, Mater. Res. Bull. 28 (1993) 1127–1134.
[35] B. Schimmoeller, H. Schulz, A. Ritter, A. Reitzmann, B. Kraushaar-Czarnetzki, A. Baiker, S.E. Pratsinis, Structure of flame-made vanadia/titania and catalytic behavior in the partial oxidation of *o*-xylene, J. Catal. 256 (2008) 74–83.
[36] R.D. Shannon, Revised effective ionic radii and systematic studies of interatomic distances in halides and chalcogenides, Acta Crystallogr. A 32 (1976) 751–767.
[37] H. Zhang, J.F. Banfield, Understanding polymorphic phase transformation behavior during growth of nanocrystalline aggregates: insights from TiO_2, J. Phys. Chem. B 104 (2000) 3481–3487.
[38] G.L. Zhao, H. Kozuka, H. Lin, T. Yoko, Sol–gel preparation of $Ti_{1-x}V_xO_2$ solid solution film electrodes with conspicuous photoresponse in the visible region, Thin Solid Films 339 (1999) 123–128.
[39] Z.M. Wang, G.X. Yang, P. Biswas, W. Bresser, P. Boolchand, Processing of iron-doped titania powders in flame aerosol reactors, Powder Technol. 114 (2001) 197–204.
[40] M.C. Heine, S.E. Pratsinis, Droplet and particle dynamics during flame spray synthesis of nanoparticles, Ind. Eng. Chem. Res. 44 (2005) 6222–6232.
[41] L. Mädler, H.K. Kammler, R. Mueller, S.E. Pratsinis, Controlled synthesis of nanostructured particles by flame spray pyrolysis, J. Aerosol Sci. 33 (2002) 369–389.
[42] F.M. Miquel, C.H. Hung, J.L. Katz, Formation of V_2O_5-based mixed oxides in flames, J. Mater. Res. 8 (1993) 2404–2413.
[43] K. Dyrek, E. Serwicka, B. Grzybowska, ESR study of the solid solutions of vanadium ions in TiO_2, React. Kinet. Catal. Lett. 10 (1979) 93–97.
[44] A. Davidson, M. Cbe, Temperature-induced diffusion of probe vanadium(IV) ions into the matrix of titanium dioxide as investigated by ESR techniques, J. Phys. Chem. 96 (1992) 9909–9915.
[45] D. Morris, R. Dixon, F.H. Jones, Y. Dou, R.G. Egdell, S.W. Downes, G. Beamson, Nature of band-gap states in V-doped TiO_2 revealed by resonant photoemission, Phys. Rev. B 55 (1997) 16083–16087.
[46] A. Vittadini, M. Casarin, M. Sambi, A. Selloni, First-principles studies of vanadia–titania catalysts: beyond the monolayer, J. Phys. Chem. B 109 (2005) 21766–21771.
[47] M.A. Larrubia, G. Busca, An ultraviolet–visible–near infrared study of the electronic structure of oxide-supported vanadia–tungsta and vanadia–molybdena, Mater. Chem. Phys. 72 (2001) 337–346.
[48] M.A. Bañares, L.J. Alemany, M.C. Jiménez, M.A. Larrubia, F. Delgado, M.L. Granados, A. Martínez-Arias, J.M. Blasco, J.L.G. Fierro, The role of vanadium oxide on the titania transformation under thermal treatments and surface vanadium states, J. Solid State Chem. 124 (1996) 69–76.
[49] S. Pilkenton, W.Z. Xu, D. Raftery, Characterization of surface and photooxidative properties of supported metal oxide photocatalysts using solid-state NMR, Anal. Sci. 17 (2001) 125–130.
[50] A.L. Linsebigler, G.Q. Lu, J.T. Yates Jr., Photocatalysis on TiO_2 surfaces: principles, mechanisms, and selected results, Chem. Rev. 95 (1995) 735–738.
[51] M. Fernández-García, A. Martínez-Arias, J.C. Hanson, J.A. Rodriguez, Nanostructured oxides in chemistry: characterization and properties, Chem. Rev. 104 (2004) 4063–4104.
[52] J.F. Zhu, F. Chen, J.L. Zhang, H.J. Chen, M. Anpo, Fe^{3+}–TiO_2 photocatalysts prepared by combining sol–gel method with hydrothermal treatment and their characterization, J. Photochem. Photobiol. A 180 (2006) 196–204.